Chinese Chemical Letters 36 (2025) 110312

Contents lists available at ScienceDirect

Chinese Chemical Letters

journal homepage: www.elsevier.com/locate/cclet

Radiation reduction modification of sp^2 carbon-conjugated covalent organic frameworks for enhanced photocatalytic chromium(VI) removal

Shouchao Zhong[a], Yue Wang[a], Mingshu Xie[a], Yiqian Wu[a], Jiuqiang Li[a], Jing Peng[a], Liyong Yuan[b,*], Maolin Zhai[a,*], Weiqun Shi[b,*]

[a] Beijing National Laboratory for Molecular Sciences, Radiochemistry and Radiation Chemistry Key Laboratory of Fundamental Science, the Key Laboratory of Polymer Chemistry and Physics of the Ministry of Education, College of Chemistry and Molecular Engineering, Peking University, Beijing 100871, China
[b] Laboratory of Nuclear Energy Chemistry, Institute of High Energy Physics, Chinese Academy of Sciences, Beijing 100049, China

ARTICLE INFO

Article history:
Received 20 May 2024
Revised 15 July 2024
Accepted 31 July 2024
Available online 3 August 2024

Keywords:
Covalent organic framework
Gamma radiation
Photocatalytic reduction
Chromium
Water purification

ABSTRACT

A sp^2 carbon-conjugated covalent organic framework (BDATN) was modified through γ-ray radiation reduction and subsequent acidification with hydrochloric acid to yield a novel functional COF (named rBDATN-HCl) for Cr(VI) removal. The morphology and structure of rBDATN-HCl were analyzed and identified by SEM, FTIR, XRD and solid-state ^{13}C NMR. It is found that the active functional groups, such as hydroxyl and amide, were introduced into BDATN after radiation reduction and acidification. The prepared rBDATN-HCl demonstrates a photocatalytic reduction removal rate of Cr(VI) above 99% after 60 min of illumination with a solid-liquid ratio of 0.5 mg/mL, showing outstanding performance, which is attributed to the increase of dispersibility and adsorption sites of rBDATN-HCl. In comparison to the cBDATN-HCl synthesized with chemical reduction, rBDATN-HCl exhibits a better photoreduction performance for Cr(VI), demonstrating the advantages of radiation preparation of rBDATN-HCl. It is expected that more functionalized sp^2 carbon-conjugated COFs could be obtained by this radiation-induced reduction strategy.

Covalent organic frameworks (COFs) are typical representatives of porous organic polymers with periodic and crystalline structures, which have wide applications in the field of photocatalysis [1,2]. Their possession of salubrious features such as high conjugated structures, low density, high stability, uniform pore distribution, and lack of metallic elements endows them with extensive potential in domains encompassing environmental conservation, energy, catalytic reactions, and detection [3-7]. Among the various COFs, sp^2 carbon-conjugated COFs (sp^2C-COFs) have garnered substantial research attention due to the following aspects: (1) sp^2C-COFs have superior stability and can be adapted to a variety of application conditions. (2) sp^2C-COFs exhibit enhanced conjugation owing to the replacement of C=N linkages with C=C linkages. Current reports suggest that sp^2C-COFs possess a broader range of light absorption compared to imine-based COFs, enabling more efficient utilization of near-infrared light. (3) sp^2C-COFs have higher separation efficiency of photoexcited electrons and holes, resulting in superior photocatalytic performance [8-12]. Despite the limited exploration of sp^2C-COFs, the above inherent structural superiority endows them with tremendous potential for photocatalytic applications.

Currently, the Knoevenagel reaction is used to synthesize sp^2C-COFs, and the resulting COFs are rich in cyanide groups. Some studies have performed amidoximation of the cyanide groups in sp^2C-COFs, which further improves the ability of COFs to recover uranium through adsorption and photocatalytic reduction synergy [13]. Additionally, there have been reports of reducing the cyanide groups of sp^2C-COFs to amino groups, optimizing their performance [14]. Through chemical modification, the cyanide groups of sp^2C-COFs can be selectively transformed into other functional groups. Compared to small molecules with good reaction activity, however, COFs as a polymer material have poor reaction activity due to their large steric hindrance [15], thereby resulting in the difficulty in the complete transformation of cyanide groups on sp^2C-COFs. That is, it is difficult to introduce sufficient functional groups onto sp^2C-COFs by the chemical modification.

* Corresponding authors.
E-mail addresses: yuanly@ihep.ac.cn (L. Yuan), mlzhai@pku.edu.cn (M. Zhai), shiwq@ihep.ac.cn (W. Shi).

https://doi.org/10.1016/j.cclet.2024.110312
1001-8417/

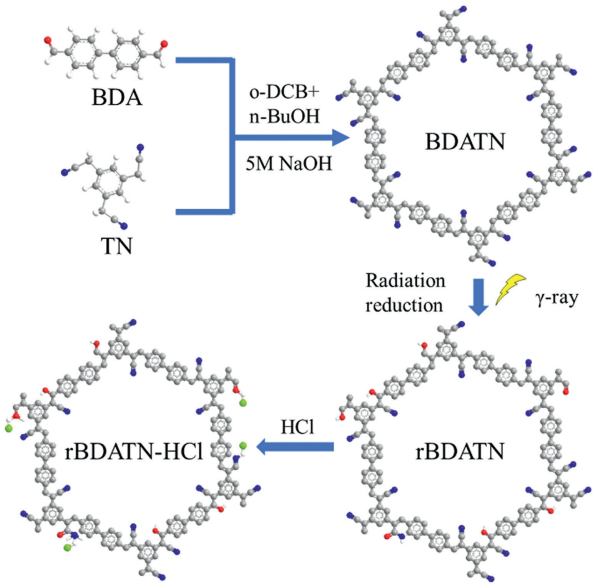

Fig. 1. Synthetic routes of BDATN, rBDATN and rBDATN-HCl with C atoms in gray, N in blue, O in red, Cl in green and H in white (H atoms in frameworks are omitted for clarity).

Radiation is a green and maneuverable material modification method. Compared to traditional chemical modification, radiation has the advantage of being efficient and controllable. In aqueous solution, gamma radiation can produce a large number of highly reactive species, such as hydrated electrons, hydrogen radicals, and hydroxyl radicals, which can effectively functionalize the materials. Through radiation modification, the functional groups have been successfully introduced into graphene, significantly improving its dispersibility [16]. Given that sp^2C-COFs have great radiation resistance due to the presence of a large number of benzene rings in the structure and their high conjugated structure [17], the functional groups can be introduced into sp^2C-COFs through radiation grafting, thereby enhancing their removal performance for charge dispersed oxoanionic pollutants, while the frameworks of the COFs remain stable [18,19].

Therefore, in this work, radiation was used to reduce a sp^2C-COF (BDATN), then the modified sp^2C-COFs, named as rBDATN-HCl, was successfully synthesized through further acidification (Fig. 1). Radiation reduction introduced active groups such as hydroxyl and amide groups into BDATN, while acidification further introduced positively charged sites, enhancing the adsorption ability of rBDATN-HCl for anions and improving its dispersibility in water. Compared to chemical reduction, radiation reduction does not require hazardous agents such as $LiAlH_4$, and the post-processing steps are simpler, making it suitable for large-scale production. To evaluate the photoreduction performance of the modified BDATN, a study on the reduction removal of Cr(VI), a common anionic environmental pollutant, was carried out, and the results showed that the photoreduction performance was greatly improved compared with the unmodified BDATN. Meanwhile, the influence of modification conditions on the properties of rBDATN-HCl and the mechanism of photocatalytic reduction for Cr(VI) were investigated in detail.

BDATN was synthesized through the Knoevenagel reaction between BDA and TN (details are given in Supporting information). The infrared spectrum (Fig. S1 in Supporting information) shows a wide vibration peak at around 1431 cm^{-1}, indicating the presence of a high conjugated structure in BDATN, while the vibration peak of the C=O (around 1688 cm^{-1}) in the reactants disappears. This confirms the successful synthesis of BDATN [13]. The rBDATN and

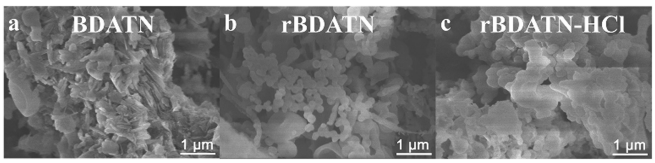

Fig. 2. SEM images of (a) BDATN, (b) rBDATN and (c) rBDATN-HCl.

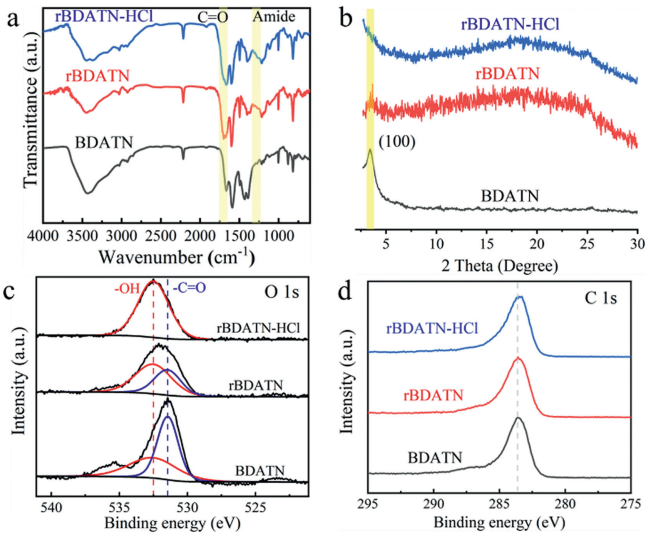

Fig. 3. Characterizations of BDATN, rBDATN and rBDATN-HCl. (a) FTIR spectra, (b) PXRD patterns, (c, d) XPS spectra of O 1s and C 1s.

rBDATN-HCl samples synthesized under different conditions were named by designating the reduction steps. The default condition was a dose rate of 10 Gy/min and an absorbed dose of 10 kGy. The names of the COFs prepared under different synthesis conditions are shown in Table S1 (Supporting information).

The SEM image (Fig. 2) shows that BDATN has a uniform nanocluster crystalline morphology. However, after radiation reduction, the crystalline morphology disappears, and the rBDATN shows a cluster morphology of mixed nanospheres and layers. In the case of rBDATN-HCl after acidification, the material underwent further agglomeration, presenting a continuous amorphous cluster morphology, indicating that the reduction and acidification had a significant effect on the morphology of BDATN.

Fig. 3a shows the changes in the infrared spectrum of BDATN after radiation reduction and acidification at 10 kGy and 10 Gy/min. After radiation reduction, the intensity of the wide vibration peak at around 1431 cm^{-1} decreases, indicating that radiation reduction reduces the conjugation of BDATN, while the vibration peak of the C=O at around 1688 cm^{-1} increases significantly, indicating that radiation reduction introduces carbonyl groups into BDATN. The vibration peak of -C≡N at around 2214 cm^{-1} after radiation reduction does not completely disappear, possibly due to the large steric hindrance and high conjugated structure of BDATN, which make it less reactive. After acidification, there is no significant change in the infrared spectrum, indicating that the structure of BDATN remains stable. In the case of acidified sample without radiation reduction (Fig. S2 in Supporting information), the intensity of the C=O vibration peak is higher, and a characteristic peak of amide appears at around 1280 cm^{-1}, indicating that some highly active cyanide groups are hydrolyzed into amides, while the active cyanides of the radiation-reduced COF are consumed by active free radicals.

The crystallinity of BDATN before and after reduction and acidification was verified by powder X-ray diffraction (PXRD, Fig. 3b).

Results showed that BDATN exhibits a strong diffraction peak at 3.4°, corresponding to its (100) crystal plane. The reduced rBDATN still exhibits a weaker diffraction peak at 3.4°, indicating that the crystallinity of BDATN still exists after radiation reduction, indicating a high radiation stability. After acidification, the disappearance of the crystal diffraction peak indicates that the crystal structure of COF vanishes. PXRD results confirm the successful synthesis of BDATN, and rBDATN retains the original crystallinity of BDATN after radiation reduction.

The ^{13}C cross-polarization magic-angle spinning (CP-MAS) NMR spectra of the prepared samples after 10 kGy and 10 Gy/min radiation reduction and acidification are shown in Fig. S3 (Supporting information). There are unreacted methylene (at around 43 ppm) and carbonyl (at around 175 ppm) groups corresponding to the monomers in BDATN. However, the free radicals produced by radiation reduction consume the methylene and carbonyl groups, and the further Knoevenagel condensation may occur [20]. In the radiation system, active species mainly consist of isopropanol radicals and hydrated electrons [21,22]. Radiation reduction results in the production of new aldehyde and amide groups through the reduction and hydrolysis of -C≡N groups (Fig. S4a and c in Supporting information), while aldehyde groups can be further reduced to hydroxyl groups (Fig. S4b in Supporting information). After acidification, the -C≡N groups are further hydrolyzed, carbonyl groups are mainly present in the form of amides (at around 170 ppm).

X-ray photoelectron spectroscopy (XPS) results show the O 1s, C 1s and N 1s XPS spectra of BDATN before and after reduction, acidification (Figs. 3c and d, and Fig. S5 in Supporting information). After radiation reduction, the binding energy of the O 1s signal significantly increases, indicating that the main form of oxygen changes from carbonyl to hydroxyl. During the irradiation process, abundant hydroxyl groups are introduced into BDATN, as shown in Fig. S6 (Supporting information). In the subsequent acidification and photocatalytic reduction of Cr(VI), there is no significant change of the O 1s signal, indicating that the hydroxyl groups are stable on the modified COF. The C 1s XPS spectrum shows that the binding energy of the C 1s signal remains unchanged, indicating that there are no significant new chemical states of carbon before and after modification, which further confirms the stability of BDATN. The N 1s XPS spectrum before and after modification also remains unchanged, indicating that the nitrogen mainly exists in the form of -C≡N or -NH_2.

Maintaining a catalyst/deionized water ratio of 1 mg/mL, BDATN, rBDATN, and rBDATN-HCl were dispersed and allowed to settle for 5 min after 5 min of ultrasonic treatment. The results show that radiation reduction and acidification can gradually improve the dispersibility of BDATN in aqueous solution (Figs. S7a-c in Supporting information). The pH of the dispersed systems was measured. Under the same conditions, the pH of deionized water is 5.89, and the pH values of the dispersed BDATN, rBDATN and rBDATN-HCl are 10.45, 9.87, and 5.33, respectively. A large number of cyanide groups in BDATN, as Lewis bases, can capture protons. Acidification can introduce rich positive charge onto the material, promote the adsorption of Cr(VI) anions, thus facilitate photocatalytic reduction. The Zeta potentials were tested in deionized water. The zeta potentials of BDATN, rBDATN and rBDATN-HCl are -38.8, -43.3, and -47.5 mV, respectively, indicating that radiation reduction and acidification introduce more Lewis base groups into BDATN. The contact angles of BDATN, rBDATN, and rBDATN-HCl were measured (Fig. S7d-f in Supporting information). Due to the strong swelling properties of COFs, all three COFs show very strong hydrophilicity.

The Mott-Schottky curves of BDATN, rBDATN, and rBDATN-HCl were measured (Figs. 4a-c). The positive slopes indicate that they are n-type semiconductors and most of the carriers are electrons [23]. Their flat-band potentials are -0.94, -0.60, and -0.90 V *vs.* NHE, respectively. Since it is generally believed that the bottom of the conduction band (CB) in many n-type semiconductors is more negative by about 0.10 V than the flat-band [24,25], the CB of BDATN, rBDATN, and rBDATN-HCl were estimated to be -1.04, -0.70, and -1.00 eV, respectively.

The band gaps of BDATN before and after radiation reduction and subsequent acidification were measured by ultraviolet-visible diffuse reflectance spectroscopy (UV-vis DRS, Fig. 4d). The results show that the light absorption range of the material becomes narrower after radiation reduction and slightly wider after acidification, but still narrower than the initial BDATN. It is attributed to the fact that the conjugation of COF decreases after radiation reduction, while acidification reintroduces electron-withdrawing groups, making the charge distribution on the material more uniform. By converting UV-vis DRS to Tauc plot (Fig. 4e), the band gaps of BDATN, rBDATN, and rBDATN-HCl are found to be 2.31, 2.42, and 2.37 eV, respectively. Combined with the conduction band potentials obtained from the Mott-Schottky curves, the valence band potentials of BDATN, rBDATN, and rBDATN-HCl are calculated to be 1.27, 1.72, and 1.37 eV, respectively. Based on the above characterizations, the energy band diagrams of BDATN, rBDATN, and rBDATN-HCl were plotted (Fig. 4f).

The photoluminescence spectrum of rBDATN is consistent with the UV-vis DRS (Fig. 5a). The maximum emission wavelength of rBDATN (528 nm) is blue-shifted by 22 nm relative to BDATN (550 nm), while the maximum emission wavelength of rBDATN-HCl (533 nm), the acidified product, is red-shifted by 5 nm relative to rBDATN (528 nm). This suggests that the conjugation of BDATN decreases after radiation reduction, and increases again after further acidification. Fig. 5b shows the transient photocurrent curves of the radiation-reduced and acidified photocatalysts, which were deposited on ITO as working electrodes and exposed to visible light. A notable decrease is observed in the transient photocurrent intensity of BDATN after radiation reduction. However, this intensity experiences a remarkable enhancement by 6.1 times after subsequent acidification, reaching a value 2.1 times greater than that of BDATN. The electrochemical impedance spectroscopy (EIS) in Fig. 5c shows that the Nyquist semicircle diameter of rBDATN is greater than that of BDATN, while the Nyquist semicircle diameter of rBDATN-HCl decreases, which is consistent with the trend of the transient photocurrent changes.

Radiation reduction was employed to obtain a series of rBDATN products at different absorbed doses and dose rates. SEM results show that with the increase of absorbed dose, the aggregation increases significantly (Figs. S8b-d in Supporting information). However, the products obtained at different dose rates exhibit similar amorphous morphology (Figs. S8e and f in Supporting information).

A series of infrared spectra of rBDATNs prepared at different absorbed doses and dose rates is found to be similar (Fig. S9a in Supporting information), indicating that absorbed dose and dose rate do not affect the types of functional group. Furthermore, UV-vis DRS and photoluminescence spectra were used to study the light absorption range and fluorescence properties of rBDATN reduced under different conditions. The results show that their UV-vis DRS and photoluminescence spectra were basically the same (Figs. S9b and c in Supporting information), indicating that absorbed dose and dose rate have little effect on the light absorption and emission properties. Comparing the O 1s XPS peak of rBDATN-HCl prepared at different absorbed doses (Fig. S9d in Supporting information), the results demonstrate a consistent O 1s signal among all rBDATN-HCl samples, primarily comprising hydroxyl groups. Furthermore, the signals for C 1s and N 1s remain unchanged. These findings suggest that the properties of the reduced product are minimally affected by the absorbed dose and dose rate. This may be due to the inert reactivity characteristic of COF as a polymer.

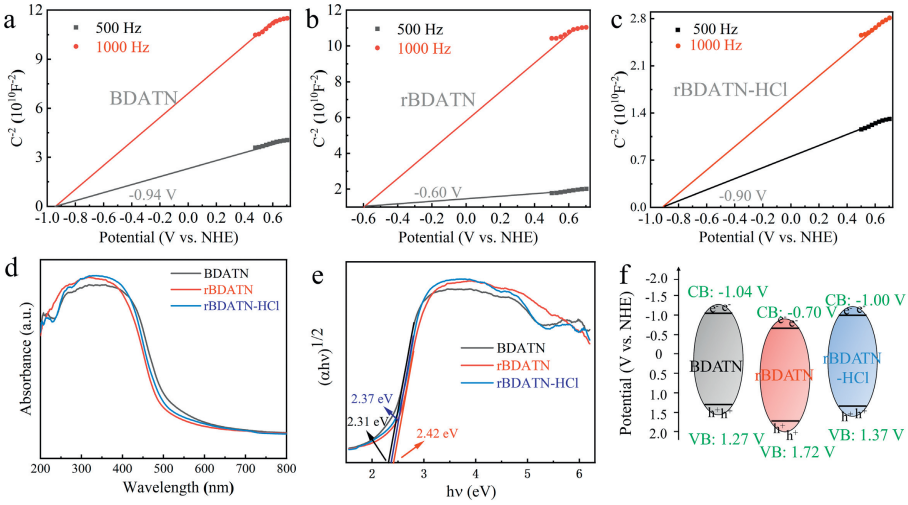

Fig. 4. Band gap analysis of BDATN, rBDATN and rBDATN-HCl. (a-c) Electrochemical Mott-Schottky curve. (d) UV-vis diffuse reflectance spectroscopy. (e) Tauc plot. (f) Band diagram.

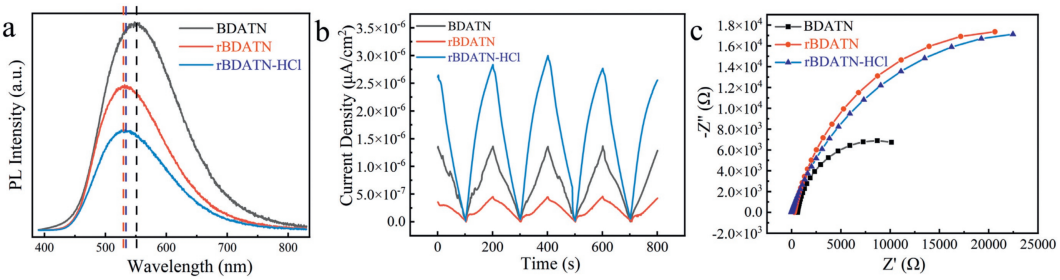

Fig. 5. Photoelectrochemical analysis of BDATN, rBDATN and rBDATN-HCl. (a) Photoluminescence spectra. (b) Transient light current corresponding spectra. (c) Electrochemical impedance spectra.

The separation of metal ions in aqueous solutions is crucial [26–28]. A series of rBDATN-HCl photocatalysts were investigated for their photocatalytic removal of Cr(VI) under visible light (≥400 nm) irradiation without any sacrificial agent. The pH of the simulated Cr(VI) wastewater was set to 3.0 [29], where Cr(VI) exists in the form of $Cr_2O_7^-$, $HCrO_4^-$, and CrO_4^{2-} [30]. The photocatalytic performance of BDATN, rBDATN and rBDATN-HCl for Cr(VI) was compared (Fig. 6a). In the dark reaction, BDATN exhibits minimal adsorption of Cr(VI) in the solution. However, rBDATN and BDATN-HCl demonstrate some adsorption capacity for Cr(VI), with the highest adsorption capacity observed in the case of rBDATN-HCl. In the light reaction, it was found that BDATN has the weakest ability to photocatalytically reduce Cr(VI), while the performance of rBDATN and BDATN-HCl demonstrates slight improvement. rBDATN-HCl exhibits the strongest photocatalytic reduction ability for Cr(VI), and can remove more than 99% of Cr(VI) in the solution within 1 h when the catalyst/solution ratio is 0.5 mg/mL. The reaction rate constants (k) of each catalyst were obtained through *pseudo*-first-order kinetic fitting ($-\ln(C/C_0) = kt$) (Fig. S10a in Supporting information). The k value of rBDATN-HCl is 0.120 min^{-1}, which is 102 times, 17 times, and 13 times higher than that of BDATN (0.00118 min^{-1}), rBDATN (0.00689 min^{-1}), and BDATN-HCl (0.00908 min^{-1}), respectively. This indicates that the modification strategy of synergistic radiation reduction and acidification is successful in enhancing the photocatalytic reduction ability of BDATN for Cr(VI). The Cr(VI) photocatalytic reduction efficiency of rBDATN-HCl is higher than the most reported COF photocatalysts in literature (Table S2 in Supporting information) [31-34].

By integrating the characterizations with the photocatalytic experimental results, a possible mechanism to explain the variations

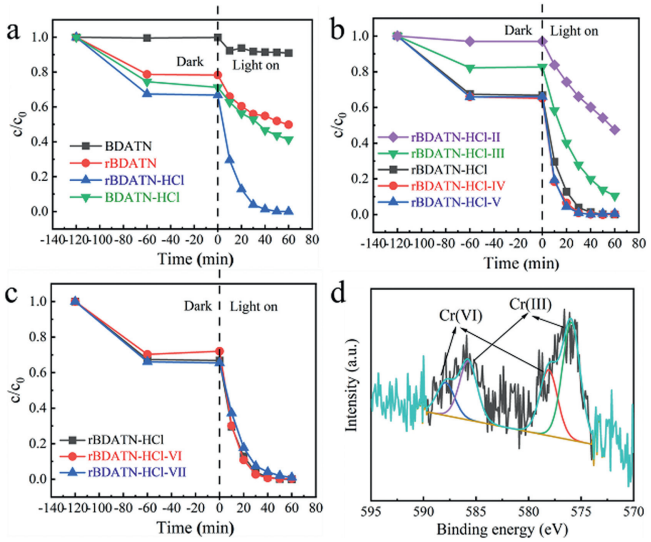

Fig. 6. The photocatalytic reduction experiments of COFs for Cr(VI). (a) Photoreduction performance of BDATN, rBDATN, rBDATN-HCl, BDATN-HCl. (b) Photoreduction performance of rBDATN-HCl synthesized at different absorbed doses and (c) at different dose rates. (d) Valence state of chromium on rBDATN-HCl after photocatalytic reduction determined by XPS.

in the photoreduction performance of BDATN after radiation reduction and acidification for Cr(VI) was proposed (Fig. S11 in Supporting information). The initial BDATN has the greatest conjugated structure with electron donor (aromatic structure) and acceptor

(-C≡N group), which facilitates the separation of photogenerated electrons and holes, thus demonstrating the minimum electrochemical impedance [35]. However, due to the lack of hydrophilic groups and the absence of active sites to capture Cr(VI) anions in the BDATN, photogenerated electrons could not be smoothly transferred to Cr(VI), resulting in the weakest photocatalytic reduction ability. After radiation reduction, the conjugation of rBDATN decreases, and some -C=C and -C≡N groups are converted into -OH groups as electron donor, which are not beneficial to the separation of photogenerated electrons and holes, resulting in a significant increase in impedance and a significant decrease in photogenerated current. However, radiation reduction also introduces a large number of electron-rich defects on BDATN, which provide abundant electrons in the photocatalytic process, and the introduction of hydroxyl groups improves the dispersibility of rBDATN in water. Therefore, rBDATN exhibits better photocatalytic reduction ability for Cr(VI) while the photochemical activity is decreased. After further acidification, rBDATN-HCl exhibits an obvious recovery in photochemical activity. This recovery is attributed to the hydroxyl groups acting as proton acceptor. Consequently, alternative donor–acceptor units are reintroduced within the material, thereby enhancing the capacity to effectively separate photogenerated electrons and holes. At the same time, after acidification, hydroxyl groups could transfer photogenerated electrons to Cr(VI) anions more effectively, and the dispersibility of the material in water is further improved. Acidification may also lead to the delamination of COF interlayers, thus enhancing its photocatalytic activity [36]. Therefore, rBDATN-HCl exhibits the strongest practical photoreduction performance for Cr(VI).

The photoreduction performance of rBDATN-HCl samples prepared at different absorbed doses for Cr(VI) was shown in Fig 6b. The results demonstrate that the rBDATN-HCl prepared with high absorbed dose has higher photoreduction performance for Cr(VI). However, when the absorbed dose exceeds 10 kGy for modification of BDATN, the photoreduction performance of the prepared rBDATN-HCl for Cr(VI) is not significantly different. This is attributed to the agglomeration caused by excessive absorbed dose (Fig. S8 in Supporting information), preventing further introduction of active functional groups. It is due to the fact that an increase in absorbed dose leads to the formation of more active functional groups and electron-rich defects into BDATN, thus favoring the photocatalytic reduction of Cr(VI). Nevertheless, when the absorbed dose exceeds 10 kGy, the limited reaction activity of BDATN prevents the introduction of more active functional groups into the COF. Additionally, rBDATN-HCl-II exhibits minimal adsorption of Cr(VI) during the dark reaction, which is possibly attributed to the fact that the free radicals consume the active -C≡N groups that could be hydrolyzed. Higher absorbed dose is required to activate the remaining -C≡N groups on the COF. rBDATN-HCl samples prepared at different dose rates demonstrate almost identical photocatalytic reduction activity for Cr(VI) (Fig. 6c), which is because dose rate has no obvious influence on the modification of rBDATN-HCl.

The reusability of rBDATN-HCl obtained by radiation reduction and acidification was investigated (Fig. S10c in Supporting information). After one cycle, the photocatalytic activity of the material slightly decreases, and the time required to completely remove Cr(VI) increases from 1 h to 2 h, but it still demonstrates stronger photocatalytic reduction activity compared to rBDATN and BDATN-HCl. It is possible that some defects in the material were consumed in the first cycle, leading to a decrease in its photocatalytic reduction activity.

XPS spectrum of rBDATN-HCl after photocatalytic reduction shows the coexistence of residual Cr(III) and Cr(VI) on the photocatalyst (Fig. 6d), proving the reduction removal mechanism of rBDATN-HCl for Cr(VI). After photocatalysis, the O 1s, C 1s, and N 1s peak positions of rBDATN-HCl remain unchanged, demonstrating the catalytic stability of rBDATN-HCl (Fig. S12 in Supporting information).

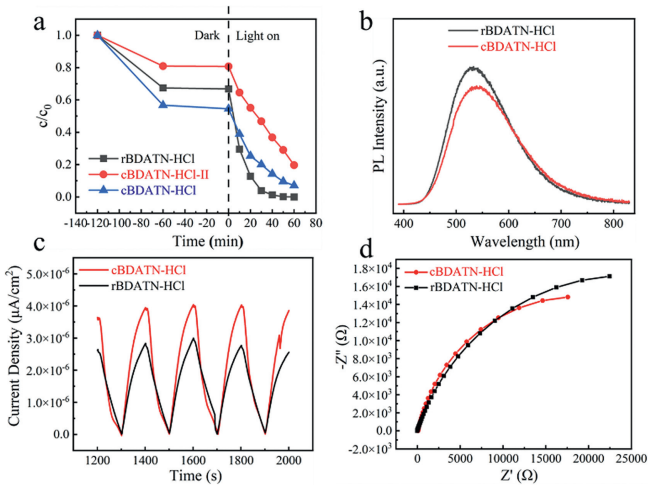

Fig. 7. Comparison of rBDATN-HCl and cBDATN-HCl. (a) photoreduction performance. (b) Photoluminescence spectra. (c) Transient light current corresponding spectra. (d) Electrochemical impedance spectra.

A detailed comparison was made between rBDATN-HCl and cBDATN-HCl modified with chemical reduction. Through chemical reduction and acidification, the conversion of -C≡N groups into ammonium groups of BDATN increases with the amount of $LiAlH_4$, resulting in an enhanced adsorption and photoreduction performance for Cr(VI) (Fig. 7a). Compared with cBDATN-HCl reduced by 60-fold equivalents $LiAlH_4$, rBDATN-HCl has weaker adsorption performance for Cr(VI). The hydroxyl and amide groups introduced by radiation reduction have weaker Lewis basicity than the amino groups introduced by chemical reduction, making it more difficult to protonate into Cr(VI) adsorption sites. However, rBDATN-HCl has stronger photoreduction performance for Cr(VI). Radiation reduction introduces more defects into BDATN, making rBDATN-HCl have stronger photocatalytic reduction activity.

The SEM images show both materials exhibit aggregation into amorphous clusters after reduction and acidification (Fig. S13 in Supporting information). As shown in Fig. S14a (in Supporting information), the infrared spectra of BDATN are not significantly changed after chemical reduction and acidification with 3 equiv. of $LiAlH_4$. However, a wide peak appears at around 3140-2710 cm^{-1} in the infrared spectra after reduction and acidification with 60 equiv. of $LiAlH_4$, corresponding to the stretching vibration peak of $-NH_2$ and $-NH_3^+$ groups, indicating that the cyanide group was converted to amino and ammonium groups in the product obtained by reduction and acidification with 60 equiv. of $LiAlH_4$. This is due to the fact that the hydrogen anion in $LiAlH_4$ has stronger selectivity towards the cyanide group in a waterless environment than the free radicals in radiation reduction. The N 1s XPS spectra of rBDATN-HCl and cBDATN-HCl were compared (Fig. S14b in Supporting information), and the N 1s signals of two samples are basically the same, representing the -C≡N group (398~400 eV) and the $-NH_2$ group (around 399 eV).

The band gap of cBDATN-HCl was measured using UV-vis DRS. It has a wider light absorption spectrum and smaller band gap compared to rBDATN-HCl (Figs. S14c and d in Supporting information), indicating that chemical reduction has a smaller impact on the conjugated structure of BDATN. Through the Mott-Schottky curve, the flat band potential of cBDATN-HCl was determined to be -0.90 V *vs.* NHE, the same as rBDATN-HCl (Fig. S14e in Supporting information). Combined with the measurement results of band

gap, the valence band potential of cBDATN-HCl was calculated to be 1.26 eV and its energy band structure was plotted (Fig. S14f in Supporting information).

The photochemical activity of rBDATN-HCl was compared with that of cBDATN-HCl. The photoluminescence spectrum indicated that the fluorescence signal of cBDATN-HCl is red-shifted compared to rBDATN-HCl (Fig. 7b). According to Figs. 7c and d, it is revealed that the transient photocurrent of rBDATN-HCl is slightly stronger than that of cBDATN-HCl, and the electrochemical impedance is slightly smaller, indicating slightly better photochemical activity.

Based on the characterizations and the photocatalytic experiments, possible differences between the two reduction methods for modification of BDATN are proposed: for chemical reduction of BDATN, the introduction of a small amount of amino groups can significantly enhance the photocatalytic reduction activity of BDATN for Cr(VI). Amino groups of BDATN can be further transformed into ammonium groups after acidification, and the positively charged COF can effectively adsorb negatively charged anions such as CrO_4^-, thus more efficiently photocatalyzing their reduction. The active species in radiation reduction of BDATN are isopropyl alcohol radicals and hydrated electrons, which have lower selectivity compared to the hydrogen anions in chemical reduction. As a result, more reduction sites on the conjugated framework of BDATN are reacted. This leads to poorer conjugation and photochemical activity of rBDATN-HCl. In addition, since radiation reduction is carried out in an aqueous system, -C≡N groups of BDATN cannot be reduced to amino groups that easily combine with protons. Therefore, in photocatalytic experiments, the rBDATN-HCl exhibits smaller adsorption capacity for Cr(VI). However, since radiation reduction introduces more electron-rich defects in the conjugated framework of BDATN, the rBDATN-HCl has more electrons that can be transferred to Cr(VI) during photocatalytic reduction, thus having stronger photoreduction performance for Cr(VI).

Research on modification of sp^2 carbon-conjugated covalent organic frameworks (COFs) is limited. In this study, we present a novel approach to modify BDATN by using radiation reduction and subsequent acidification, resulting in the creation of a green photocatalyst, rBDATN-HCl. Without any sacrificial agents, rBDATN-HCl could remove more than 99% of Cr(VI) within 60 min under visible light, with a catalytic reaction rate constant 102 times greater than that of unmodified BDATN. Characterizations demonstrated that the radiation reduction and acidification introduced active functional groups, such as hydroxyl and amide, into BDATN, thereby enhancing its dispersibility in water and adsorption capacity for Cr(VI). Moreover, compared with cBDATN-HCl, which was obtained *via* chemical reduction and acidification, rBDATN-HCl exhibited superior photoreduction performance for Cr(VI), thus highlighting the effectiveness of the green radiation modification strategy.

Declaration of competing interest

The authors declare that they have no known competing financial interests or personal relationships that could have appeared to influence the work reported in this paper.

CRediT authorship contribution statement

Shouchao Zhong: Writing – original draft, Validation, Investigation, Conceptualization. **Yue Wang:** Writing – review & editing. **Mingshu Xie:** Writing – review & editing. **Yiqian Wu:** Writing – review & editing. **Jiuqiang Li:** Resources. **Jing Peng:** Writing – review & editing. **Liyong Yuan:** Writing – review & editing, Supervision. **Maolin Zhai:** Writing – review & editing, Supervision, Resources, Funding acquisition. **Weiqun Shi:** Writing – review & editing, Supervision, Funding acquisition.

Acknowledgments

This work was supported by the National Natural Science Foundation of China (No. U2067212) and the National Science Fund for Distinguished Young Scholars (No. 21925603).

Supplementary materials

Supplementary material associated with this article can be found, in the online version, at doi:10.1016/j.cclet.2024.110312.

References

[1] S. Deng, T. Yan, M. Wang, et al., Supramol. Mater. 2 (2023) 100034.
[2] M. Zhu, J. Chen, Y. Lin, Supramol. Mater. 2 (2023) 100030.
[3] S. Lin, C.S. Diercks, Y.B. Zhang, et al., Science 349 (2015) 1208–1213.
[4] H. Wei, X. Li, F. Huang, et al., Chin. Chem. Lett. 34 (2023) 108564.
[5] H. Wang, H. Ding, X. Meng, C. Wang, Chin. Chem. Lett. 27 (2016) 1376–1382.
[6] L. Ma, S. Wang, X. Feng, B. Wang, Chin. Chem. Lett. 27 (2016) 1383–1394.
[7] M.X. Wu, Y.W. Yang, Chin. Chem. Lett. 28 (2017) 1135–1143.
[8] J.L. Shi, R. Chen, H. Hao, C. Wang, X. Lang, Angew. Chem. Int. Ed. 59 (2020) 9088–9093.
[9] Y. Zhao, H. Liu, C. Wu, et al., Angew. Chem. Int. Ed. 58 (2019) 5376–5381.
[10] E. Jin, Z. Lan, Q. Jiang, et al., Chem 5 (2019) 1632–1647.
[11] F. Zhang, Y. Wang, H. Zhao, et al., ACS Appl. Mater. Interfaces 16 (2024) 8772–8782.
[12] Q. Guo, H. Ji, L. Yang, et al., Chin. Chem. Lett. 33 (2022) 2621–2624.
[13] W.R. Cui, F.F. Li, R.H. Xu, et al., Angew. Chem. Int. Ed. 59 (2020) 17684–17690.
[14] X. Guan, H. Li, Y. Ma, et al., Nat. Chem. 11 (2019) 587–594.
[15] J. Li, X. Yang, C. Bai, et al., J. Colloid Interface Sci. 437 (2015) 211–218.
[16] Y.W. Zhang, H.L. Ma, J. Peng, M.L. Zhai, Z.Z. Yu, J. Mater. Sci. 48 (2013) 1883–1889.
[17] L. Zhu, D. Sheng, C. Xu, et al., J. Am. Chem. Soc. 139 (2017) 14873–14876.
[18] Y. Wang, M. Xie, J. Lan, et al., Chem 6 (2020) 2796–2809.
[19] Y. Wang, J. Lan, X. Yang, et al., Adv. Funct. Mater. 32 (2022) 2205222.
[20] M. Zhang, J. Chen, S. Zhang, et al., J. Am. Chem. Soc. 142 (2020) 9169–9174.
[21] S. Li, X. Que, X. Chen, et al., ACS Appl. Energy Mater. 3 (2020) 10882–10891.
[22] X. Que, T. Lin, S. Li, et al., Appl. Surf. Sci. 541 (2021) 148345.
[23] S. Bi, C. Yang, W. Zhang, et al., Nat. Commun. 10 (2019) 2467.
[24] F. Zhang, J. Sheng, Z. Yang, et al., Angew. Chem. Int. Ed. 57 (2018) 12106–12110.
[25] F. Xu, C. Lai, M. Zhang, et al., J. Colloid Interface Sci. 601 (2021) 196–208.
[26] X. Li, Q. Wu, C. Wang, et al., Chin. Chem. Lett. 35 (2024) 109359.
[27] T. Xiu, S. Zhang, P. Ren, et al., Chin. Chem. Lett. 34 (2023) 108440.
[28] L. Su, Q. Wu, C. Wang, J. Lan, W. Shi, Chin. Chem. Lett. 35 (2024) 109402.
[29] A. Dzieniszewska, J. Kyziol-Komosinska, M. Pajak, Peer J. 8 (2020) e9324.
[30] S.J. Wang, H.L. Ma, J. Peng, et al., Dalton Trans 44 (2015) 7618–7625.
[31] Y. Zhang, H. Ye, D. Chen, et al., J. Membr. Sci. 628 (2021) 119216.
[32] F. Liu, Z. Ma, Y. Deng, et al., Environ. Sci. Technol. 55 (2021) 5371–5381.
[33] H. Zhang, L. Zhang, S. Dong, et al., J. Hazard. Mater. 446 (2023) 130756.
[34] S. Zhong, Y. Wang, S. Li, et al., Sep. Purif. Technol. 294 (2022) 121204.
[35] J. Li, S. Gao, J. Liu, et al., Adv. Funct. Mater. 33 (2023) 2305735.
[36] D.W. Burke, C. Sun, I. Castano, et al., Angew. Chem. Int. Ed. 59 (2020) 5165–5171.